WPMST1-PR(18) 21286

M Dimitrova et al.

EEDF in the COMPASS divertor region during an impurity-seeding experiment

Preprint of Paper to be submitted for publication in
Nuclear Fusion

This work has been carried out within the framework of the EUROfusion Consortium and has received funding from the Euratom research and training programme 2014-2018 under grant agreement No 633053. The views and opinions expressed herein do not necessarily reflect those of the European Commission.

EEDF in the COMPASS divertor region during an impurity-seeding experiment

M Dimitrova[1,2], Tsv K Popov[2,3], M Komm[1], J Kovacic[4], R Dejarnac[1], P Ivanova[2], J Stöckel[1], V Weinzettl[1], P Vondracek[1,5], P Hacek[1], M Hron[1], R Panek[1], the COMPASS team and the EUROfusion MST1 Team[6]

[1] Institute of Plasma Physics, The Czech Academy of Sciences, Za Slovankou 3, 182 00 Prague 8, Czech Republic
[2] Emil Djakov Institute of Electronics, Bulgarian Academy of Sciences, 72, Tsarigradsko Chaussee, 1784 Sofia, Bulgaria
[3] Faculty of Physics, St. Kliment Ohridski University of Sofia, 5, J. Bourchier blvd., 1164 Sofia, Bulgaria
[4] Jožef Stefan Institute, 39, Jamova, 1000 Ljubljana, Slovenia
[5] Faculty of Mathematics and Physics, Charles University in Prague, Prague, The Czech Republic
[6] See authors list in H. Meyer et al., Nuclear Fusion 57 102014 (2017)

[*]E-mail: dimitrova@ipp.cas.cz

Abstract. This work presents results from swept Langmuir probe measurements in the divertor region of the COMPASS tokamak in D-shaped, L-mode deuterium discharges. The electron energy distribution function (EEDF) was studied during a detachment experiment with nitrogen and neon injected into the divertor region.
The current-voltage probe characteristics measured were processed using the first-derivative probe technique, which allows one to evaluate the plasma potential and the real electron energy distribution function (respectively, the electron temperature and density).
In the divertor region of the COMPASS tokamak, the EEDF of the attached plasma usually deviates from Maxwellian, but it can be approximate by a sum of two Maxwellian distributions (bi-Maxwellian EEDF) with a low-energy electron population with temperatures 3.5-5 eV and a high-energy electron group with temperatures 10-25 eV.
During the nitrogen seeding, the EEDF changes to Maxwellian with temperatures 3.5-7 eV. The hypothesis is discussed that the fast electrons relax via inelastic collisions with N_2 and a Maxwellian EEDF is thus formed.
The poloidal profiles of the plasma potential, electron temperatures and densities are presented, together with the parallel power-flux density distribution, in the divertor region of the COMPASS tokamak before and during the impurity seeding.

1. Introduction

The reduction of the heat load on the divertor target is crucial for the ITER and next-step fusion devices. The need to reduce it to an acceptable level triggered intense theoretical and experimental studies of the physics of divertor plasma detachment [1]. One way to reach detachment is impurity seeding; studies in this respect started more than 30 years ago in many tokamaks, such as ASDEX [2], JT-60U [3], JET [4, 5], Alcator C-Mod [6] etc. These efforts notwithstanding, most of the studies on power deposition in contemporary tokamaks have been performed in attached plasmas [7] because the detached regimes tend to be more difficult to diagnose: The principal diagnostic technique for power load studies is infrared thermography, witch suffers from interference caused by increased

bremsstrahlung in the infrared spectrum in detached plasmas. The tokamak COMPASS [8] has an open divertor geometry and a short connection length to the target and is, thus, considered as unfavorable for the detached regime, which is usually achieved by employing impurity seeding in the divertor region.

On the other hand, it is known that a partial detachment is considered to be a mandatory regime for ITER operation [1]. This is why we recently started a series of experiments with nitrogen and neon impurity injection at different locations in the COMPASS divertor with the aim to influence the particle and heat transport in the divertor region, thus provoking a partial detachment. The effects on scrape-off layer (SOL) and divertor plasma conditions were monitored by means of a horizontal reciprocating probe located at the outer midplane and by old [9, 10, 11] and new divertor Langmuir and Ball-pen probe arrays [12]. The radiation in the edge plasma was observed by AXUV bolometers and fast visible-light cameras; the first results were reported in [13].

This paper reports a continuation of our experimental study on impurity seeding in D-shaped, L-mode, deuterium plasmas. We studied the properties of the plasma in the divertor region before and during nitrogen and neon seeding by means of the divertor probe system in the COMPASS tokamak [8]. The current-voltage (*IV*) probe characteristic measured were processed by the advanced first-derivative probe technique (FDPT) [14], which provides information on the poloidal distribution of the plasma potential and the real electron energy distribution function (EEDF), respectively, the electron temperatures and densities. Using these data, the parallel power-flux density distribution was calculated [10, 15, 16] in the divertor region of the COMPASS tokamak before and during the impurity seeding.

2. Experimental set-up and probe technique for divertor plasma studies

Nitrogen and neon were injected at varying amounts in a series of otherwise identical ohmic L-mode discharges with I_{pl} = 210 kA, line-average electron density $n_e^{aver} = 4\times10^{19}$ m^{-3} and toroidal magnetic field $B_T = -1.38$ T. Nitrogen was introduced into the vessel through a pre-programmed piezo-valve in a toroidal location R = 0.469 m in the private flux region (PFR). The valve was connected to a gas reservoir at a pressure of 2.1 bar. The waveform of the gas puff had two parts: a short 10 ms full opening of the valve, which ensured that the valve was not stuck, followed by 100 ms injection at flow levels varying between 2.0×10^{20} and 4.5×10^{20} molecules per second.

Another series of experiments with nitrogen and neon gas puff using a valve in the divertor on the low-field side (LFS) (R = 0.500 m**),** was also performed and analyzed. In figure 1 we present an example of the main plasma parameters of discharge #15975 with nitrogen seeding on the LFS (indicated by a yellow line). The line-average electron density measured by the interferometer is presented by a magenta line and the Thomson scattering laser diagnostic results, by a blue one. The injection was monitored by a fast visible-light RIS1 camera [17], which clearly showed the formation of an emissive ring in the divertor (see figure 2).

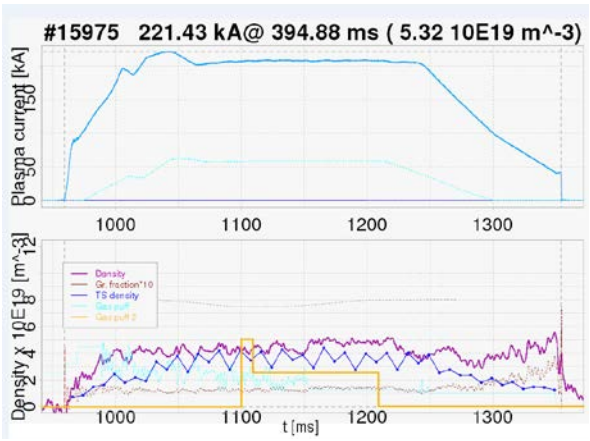

Figure 1. Main plasma parameters of discharge #15975.

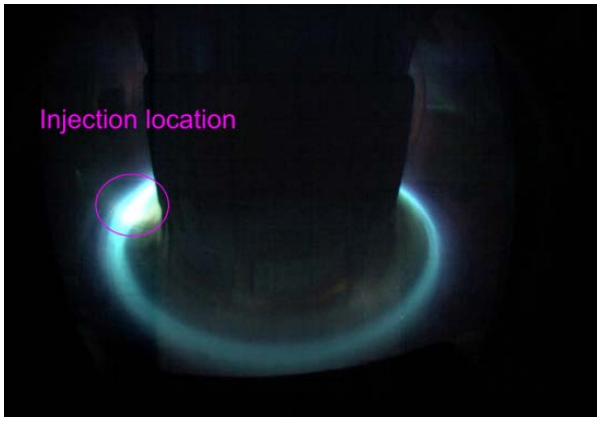

Figure 2. Formation of the radiative ring during nitrogen gas puff as seen by a fast visible-light camera.

The divertor probe system in use in the COMPASS tokamak consists of 39 single graphite Langmuir probes (LP) embedded poloidally in the divertor tiles providing data with a 5-mm spatial resolution [10]. The probes were biased with respect to the tokamak chamber wall by a swept triangular voltage U_{pr} with a frequency of 1 kHz [18], and the probe current and voltage versus time were recorded by the COMPASS DAQ. From these data, the *IV*s were constructed and further processed to estimate the main plasma parameters – plasma potential and EEDF, respectively, the electron temperatures and densities.

In strongly magnetized fusion plasma, the electron part of the *IV* characteristics above the floating potential is strongly distorted due to the influence of the magnetic field – as the magnetic field increases, the electron branch is gradually depressed. Therefore, in fusion plasmas, the ion saturation branch of the *IV* characteristics and the part around the floating potential are usually used when retrieving the electron temperature and density [19, 20]. This conventional technique assumes a Maxwellian EEDF but in fact does not measure the real one.

However, there appeared theoretical predictions [21-23] and experimental evidence [10, 24, 25] that the EEDF can deviate from the Maxwellian in the divertor region of tokamaks, namely, the presence of a large number of low-temperature electrons predominating over a group of high-temperature electrons. It should be emphasized that the conventional probe techniques using the ion saturation branch of the *IV* characteristics measured and the part around the floating potential can estimate only the temperature of the high-energy electron fraction of the bi-Maxwellian distribution.

This is why, to obtain the real EEDF from the measured *IV* probe characteristics, the advanced first-derivative probe technique (FDPT) was used in this work, as presented and discussed in detail in [15]. Figures 3 and 4 below illustrate examples of the results obtained by measurements with LP #12 (position 0.4421 m, shot #13730, N_2 seeding rate 3.7×10^{20} s^{-1}) before and after nitrogen seeding The figures present the electron energy probability function (EEPF), $f(\varepsilon)$, which provides the same information as the EEDF $F(\varepsilon) = f(\varepsilon)\sqrt{\varepsilon}$: When presented on a semi-log scale, the EEPF is a straight line for a Maxwellian distribution, which allows for easier approximations with model functions when the EEDF differs from Maxwellian [26].

Figure 3 presents the EEPF at time 1100 ms just before nitrogen puffing. It is clearly seen that the EEDF is not Maxwellian, but can be approximated by a sum of two Maxwellian EEDFs – one low-energy electron group with temperature $T_e^l = 3.5 \pm 0.2$ eV and density $n_e^l = (5.0 \pm 0.5)\times10^{21}$ m^{-3}, and a second one with a higher energy, with $T_e^h = 11 \pm 1$ eV and density $n_e^h = (3.3 \pm 0.8)\times10^{21}$ m^{-3}. The estimated plasma potential is $U_{pl} = 39 \pm 3$ V.

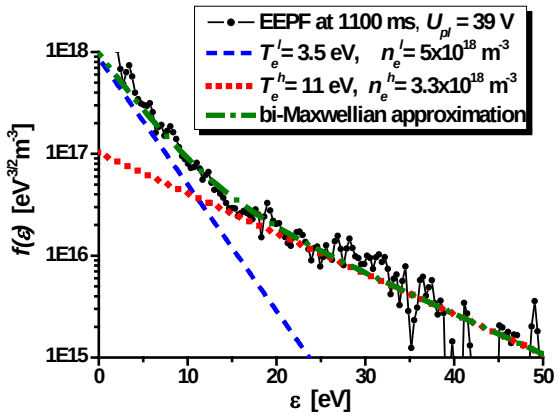

Figure 3. Experimental EEPF (line-dot) before nitrogen seeding – a low-energy electron group (dashed line), and a second one with higher energy (dotted line). The bi-Maxwellian approximation is presented with dash-dotted line.

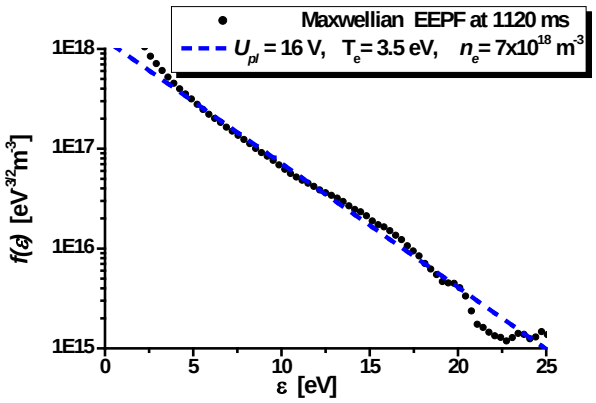

Figure 4. Experimental EEPF (dots) during nitrogen seeding. It can be approximated by a straight (dashed) line, i.e. the EEDF is Maxwellian.

The origin of the bi-Maxwellian EEDF in figure 3 is discussed in [17, 27]. Particles and energy are introduced in the SOL mainly through transport in form of blobs; the latter being filamentary structures formed behind the separaterix in the edge plasma due to the large temperature and density gradients, the result of which is the turbulent nature of the transport in this region. The charge separation occurring as a result of the B x grad B drift from the non-uniformity of the magnetic field in the edge region leads to expulsion of the filaments into the SOL and radially outwards towards the wall. The filaments enter the SOL in a region poloidally roughly ±30 ° around the outer midplane and then propagate in the parallel and radial direction towards the divertor and the wall, respectively.

The parallel conductivity is much greater, especially for the electrons, so the fast electrons from the tail of the EEDF try to connect rapidly to the divertor plates. The probability for them actually reaching the divertor with a high energy depends on the SOL collisionality. As we have shown in [11], at lower densities and on the outer target (a shorter connection length) there is a higher number of fast particles whose energy is sufficient to ionize the neutrals in the divertor region. Consequently, they then discretely lose their energy through inelastic collisions, which creates two distinct energy groups of electrons that we detect as a bi-Maxwellian EEDF.

The results in [11] also show that at high densities, when the fueling is increased, the EEDF relaxes into Maxwellian in the entire divertor region due to collisions, which is followed by a partial detachment. Seeding with an impurity having a higher cross-section of inelastic collisions with electrons [29] promotes the transition to a partial detachment mode at a lower line-average electron density, which is the main goal of this study.

An example of the EEPF obtained during nitrogen seeding is presented in figure 4. The EEDF is Maxwellian with $T_e = 3.5 \pm 0.2$ eV and density $n_e = (7.0 \pm 0.7) \times 10^{21}$ m^{-3}. The plasma potential is $U_{pl} = 16 \pm 2$ V.

3. Experimental results and discussion

3.1 Poloidal profiles of the plasma parameters during nitrogen seeding

Below we present experimental results of the poloidal distribution of the plasma parameters before and during nitrogen seeding at different rates in the PFR and the LFS in the divertor region of the COMPASS tokamak. In the figures, the different colors correspond to different amounts of gas seeded in the divertor region – from 2.0×10^{20} to 4.5×10^{20} molecules N_2 per second.

When the valve was on the LFS, the discharges were stable and lasted longer. When the seeding was in the PFR, with the number of molecules as low as 4.5×10^{20} s^{-1}, the discharge was shorter and ended with a disruption.

Figure 5 presents poloidal profiles of the floating (a, b) and plasma potentials (c, d) before and during seeding with different amounts of N_2. On the left-hand side, the results are presented when the seeded gas was puffed in the PFR at 1160 ms during the discharges; the right-hand part presents results when the puff was on the LFS at time 1145 ms. The positions of the strike points are indicated hereinafter by vertical dashed lines.

When the N_2 gas puff was from a valve placed on the divertor's PFR, in the high-field side (HFS) region of the divertor, even the smallest amount of gas changed the floating potential U_{fl} significantly (figure 5 a). In the divertor's LFS region, the negative floating potential decreased in absolute values gradually as the nitrogen seeding was raised. In contrast, when the nitrogen was puffed on the LFS, the floating potential on the divertor's HFS region decreased gradually with the increase of the amount of gas puffed (figure 5 b). On the divertor's LFS, a significant change was only observed when 4.4×10^{20} N_2 molecules per second were seeded.

The changes in the plasma potential U_{pl} are presented in figures 5 c and d. The plasma potential changes its sign, from naturally positive on the HFS to zero and even negative on the LFS. Similar results were obtained in COMPASS-D and reported in [32]. We assume that, most likely, this is caused by the thermoelectric current [30] with the non-Maxwellian feature of the EEDF – due to the different connection length on the HFS and effects of drifts, the temperature of the high-energy group of electrons is lower than on the LFS side. The subsequent currents are also closed over the divertor tiles. The negative potential established most likely forms an electron-rich sheath in front of the divertor, which should be carefully taken into account when predicting the heat loads on the surface.

When nitrogen was puffed by the PFR valve, the plasma potential value decreased rapidly on the HFS and did not change significantly in the entire divertor region as the amount of the gas puffed was further increased (figure 5 c).

When the seeding was inserted in the LFS (figure 5 d), the tendency of the plasma potential variation on the divertor's HFS was the same above 2.6×10^{20} s^{-1} N_2 gas puff – the plasma potential value decreased rapidly. In contrast, a significant change on the LFS was only observed when the N_2 gas puff was 4.4×10^{20} s^{-1}.

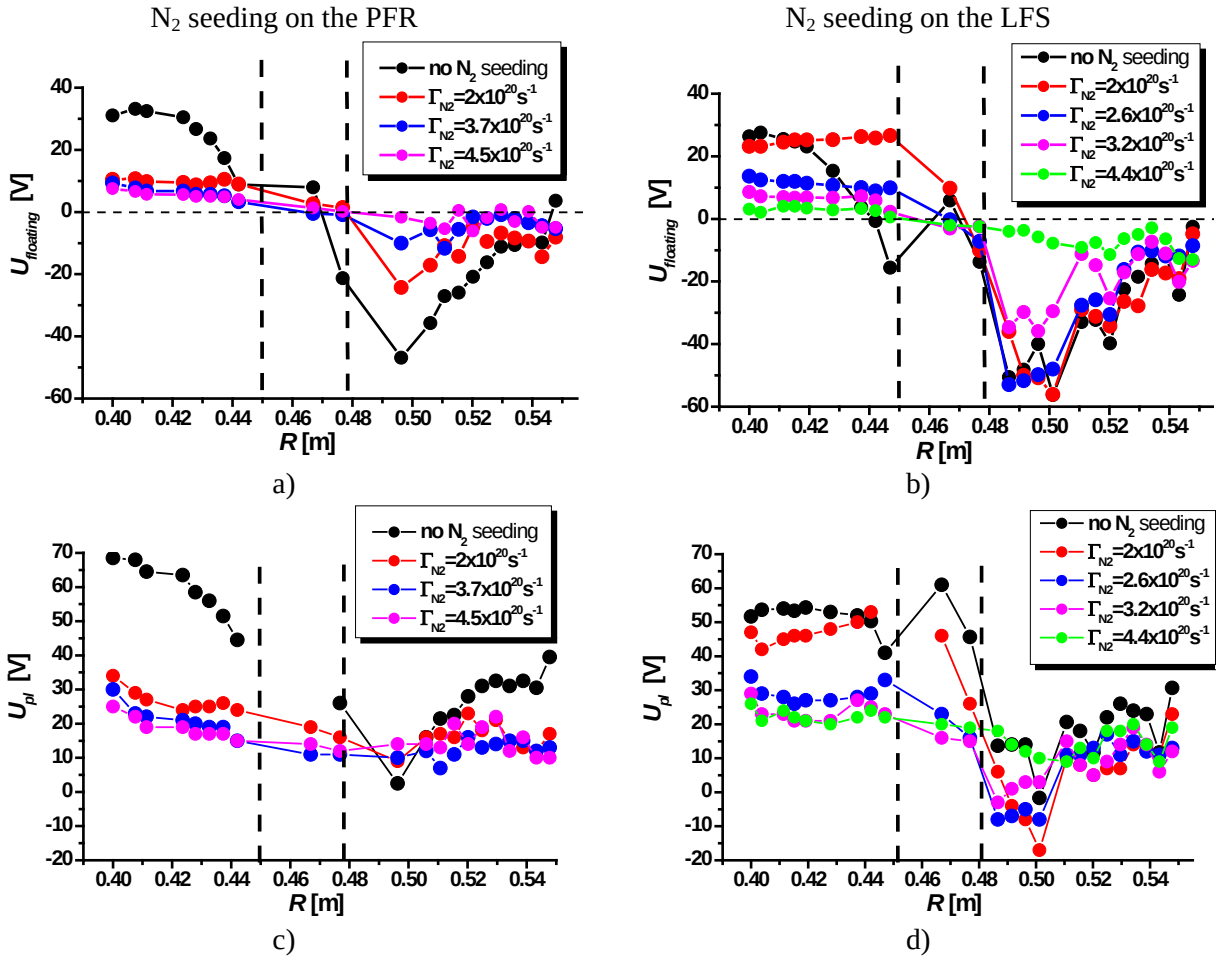

Figure 5. Poloidal profiles of the floating and plasma potentials during seeding on the PFR (a, c) and on the LFS (b, d) with different amounts of N_2 molecules per second.

Figure 6 presents poloidal profiles of the ion saturation current density J_{sat} before and during seeding in the PFR (a) and on the LFS (b) with different number of N_2 molecules per second. When the seeding was in the PFR, a sharp drop of the J_{sat} values, especially in the vicinity of the outer strike point, was observed. The poloidal profiles were almost flat and practically coincided when the seeding was at the rates of 3.7×10^{20} s^{-1} and 4.5×10^{20} s^{-1}. When the seeding was on the LFS, the J_{sat} value decreased gradually and the peak of the J_{sat} on the outer strike point disappeared at 4.4×10^{20} s^{-1} N_2 seeding.

Figure 7 shows the poloidal profiles of the electron temperatures before and during N_2 seeding in the PFR (a) and on the LFS (b) with different number of molecules per second. The EEDF was bi-Maxwellian in attached plasmas before the seeding; the two groups of electrons are shown in figure 7 a) and b). Here and further on, the low-temperature group is denoted by triangles, and the high-temperature one, by squares. When the EEDF is Maxwellian, the electron temperature is presented by empty circles.

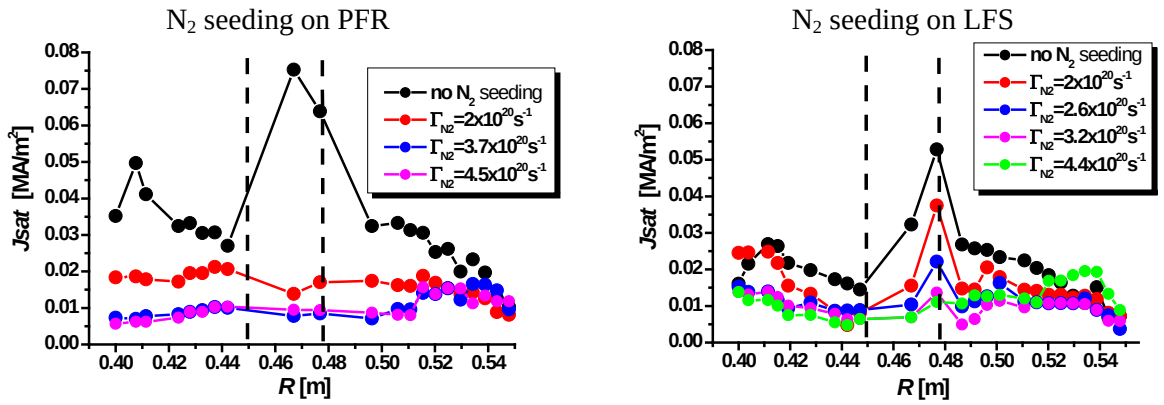

a) b)

Figure 6. Poloidal profiles of the ion saturation current density before and during N_2 seeding in the PFR (a) and on the LFS (b) with different number of molecules per second.

Before the N_2 seeding, the EEDF was bi-Maxwellian with a low-energy electron fraction with $T_e^l \approx 3.5$ eV, and a higher-energy one with temperatures T_e^h in the interval from 10 eV to 22 eV. During the N_2 seeding at 2×10^{20} s^{-1} through a valve in the PFR, the EEDF was Maxwellian in the HFS and in the private flux region, while in the LFS divertor region it was bi-Maxwellian. At 3.7×10^{20} s^{-1} and 4.5×10^{20} s^{-1} nitrogen puff, the EEDF was Maxwellian everywhere (figure 7 a) with electron temperatures between 3.5 eV and 7 eV.

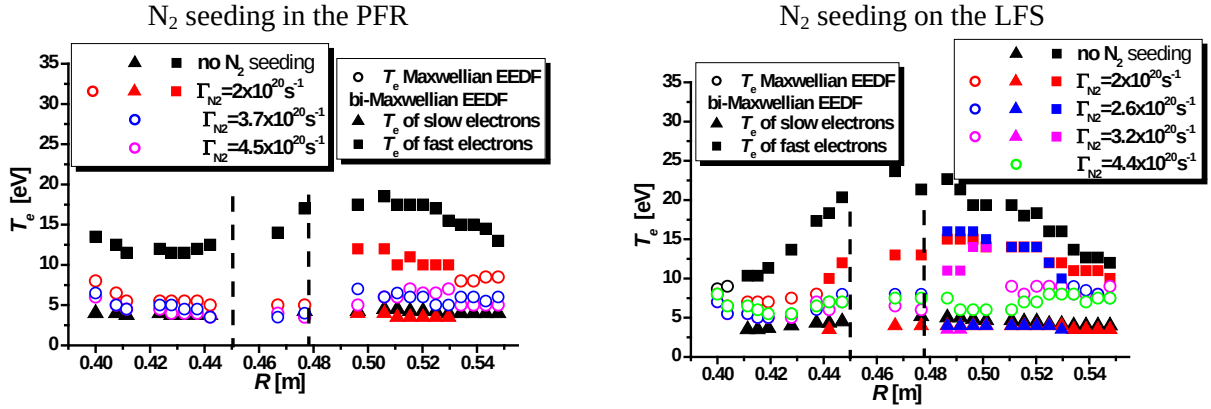

a) b)

Figure 7. Poloidal profiles of the electron temperatures before and during N_2 seeding in the PFR (a) and on the LFS (b) with different number of molecules per second.

When N_2 was puffed at 2×10^{20} s^{-1} on the LFS (red color in figure 7 b), the EEDF was bi-Maxwellian around the inner and outer strike points, PFR and LFS. When the seeding used was 2.6×10^{20} s^{-1} (blue symbols), the EEDF was bi-Maxwellian only on the LFS, 5 cm away from the OSP. In contrast, seeding with N_2 at a rate of 4.4×10^{20} s^{-1} (the green circles) resulted in a Maxwellian EEDF in the entire divertor region with electron temperatures between 5 eV and 7.5 eV.

Figure 8 shows the electron densities n_e obtained for 2×10^{20} s^{-1} and 4.5×10^{20} s^{-1} of N_2 seeding. The same symbols as for the temperatures are used, and comparisons with the densities before N_2 seeding (black signs) are presented. In general, the effect of seeding was stronger on the HFS, namely, a decrease of the total electron density. This corresponds also with the poloidal profiles of J_{sat} (figure 6), where a decrease is also seen.

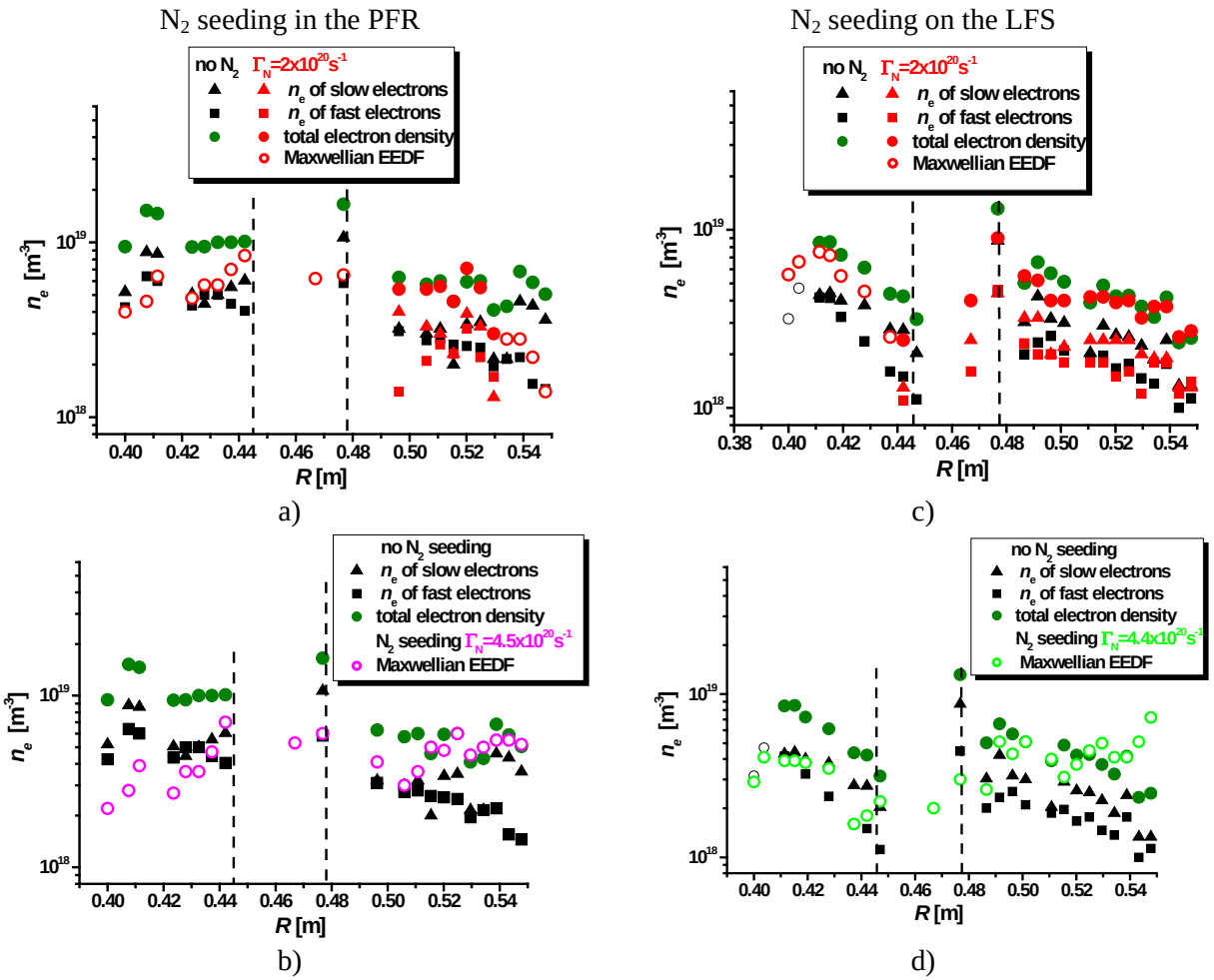

Figure 8. Poloidal profiles of the electron densities before N_2 seeding presented in every plot with black symbols. The results obtained during N_2 seeding in the PFR (a, b) and on the LFS (c, d) with similar numbers of molecules per second are presented by the same colors as in figure 7.

There is a difference in the time evolution of the transition from bi-Maxwellian to Maxwellian EEDF during N_2 seeding in the PFR (at 3.7×10^{20} s^{-1}) and on the LFS (at 3.2×10^{20} s^{-1} nitrogen puff). Figure 9 illustrates the temporal profiles of the electron temperatures obtained by LP#9 (R = 0.4279 m) and LP#23 (R = 0.4963 m). Both are located at the same distance of 1.6 cm to the left from the inner strike point and to the right from the outer strike point.

When the seeding was by the valve in the PFR, the duration of the transition from bi-Maxwellian to Maxwellian EEDF was about 10 – 15 ms in both HFS and LFS divertor regions. Unfortunately, in this case the bolometric diagnostic [31] show that the seeded N_2 penetrated in the confined plasma and cooled it, as evidenced by the high-resolution Thomson scattering [9]. This is why, as it was mentioned before, when the N_2 is seeded in the PFR, the discharges are shorter and often end with disruption.

When N_2 seeding was by a LFS valve, the transition from bi-Maxwellian to Maxwellian EEDF took longer – 25 – 45 ms. Radiation was observed [31] in both HFS and LFS simultaneously, the nitrogen remained in the divertor, but also penetrated the LFS plasma edge.

The considerations above show that although the Maxwelization of the electrons is faster in the case of PFR seeding, the LFS seeding is more effective in achieving a stable partial-detachment in the COMPASS tokamak.

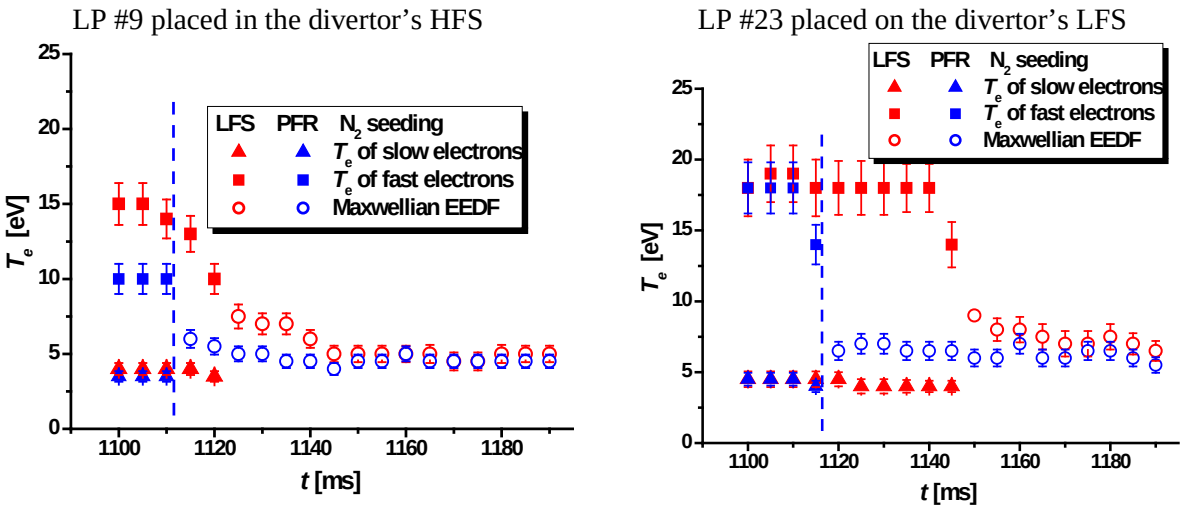

Figure 9. Temporal profiles of the electron temperatures obtained by LP#9 (a) and LP#23 (b) during N_2 seeding by 3.7×10^{20} molecules per second.

In what concerns the transition from attached to a partially-detached plasma in the divertor region in the COMPASS tokamak, the existence of a bi-Maxwellian EEDF before N_2 seeding and the formation of a Maxwellian EEDF during seeding needs a more detailed discussion. The decrease of the electron temperature below 5 eV in the divertor region is one of the indications of detached plasma operation, as well as of a reduced flow of charged particles to the divertor strike points [30]. The peaks in the poloidal profiles of the electron temperature T_e and ion saturation current density J_{sat} measured around the strike points disappear during the seeding [1-5], which is considered as evidence of a transition from attached to partially-detached plasma.

When the detachment mode is studied by means of Langmuir probes, the electron temperature is usually estimated from *IV* probe characteristics measured using the conventional 3-parameter technique or triple probe technique. As mentioned in section 2 above, this techniques can only estimate the temperature of the high-energy electron fraction of the bi-Maxwellian EEDF, even if it is less populated in comparison with the dominating low-temperature electron fraction. When an impurity is seeded, the electrons from the higher-energy group lose some of its energy due to inelastic collisions with the impurity. These electrons, together with the more populated low-energy electron group, form a Maxwellian EEDF with a somewhat higher electron temperature. In other words, when the EEDF is bi-Maxwellian before impurity seeding, during the seeding a Maxwellian EEDF is formed. But, should the presence of the most populated low temperature electron group not be taken into account, which happens when the conventional probe technique is used, an ostensible significant cooling of all plasma electrons would incorrectly be observed.

Bearing the above in mind, one should interpret more carefully the results of the electron temperature measurements. Thus, when studying using Langmuir probes the transition from attached to detached plasma operation induced by impurity seeding, one should account for the fact that the real EEDF deviates from Maxwellian. This also affects the calculation of the parallel power-flux density in the divertor region. In [16], the estimation of the heat transition coefficient γ in the case of bi-Maxwellian EEDF is discussed in detail. We have to point out that when the EEDF is bi-Maxwellian, one should use an effective electron temperature $T_e^{eff} = \frac{T_e^h T_e^l (n_e^l + n_e^h)}{n_e^h T_e^l + n_e^l T_e^h}$ [16] to calculate the parallel power-flux density.

Using the data presented in figures 6, 7 and 8, the poloidal profiles of the parallel power-flux density are calculated and presented in figure 10. When the EEDF is Maxwellian, the heat transition coefficient γ is assume as 7.5. When the EEDF is bi-Maxwellian, it varies between 12 and 18. It is seen the N_2 seeding, results in a practically flat distribution in the divertor region at higher amounts of seeded molecules. The value of the parallel power-flux density in the central area of the divertor drops by about one order of magnitude and the peaks around the strike points disappear. We avoided

calculating the parallel heat flux at the points where the plasma potential in front of the divertor is negative. In this case, the electron-rich sheath demands a different kind of treatment to estimate the heath fluxes, which we intend to look into in a future work.

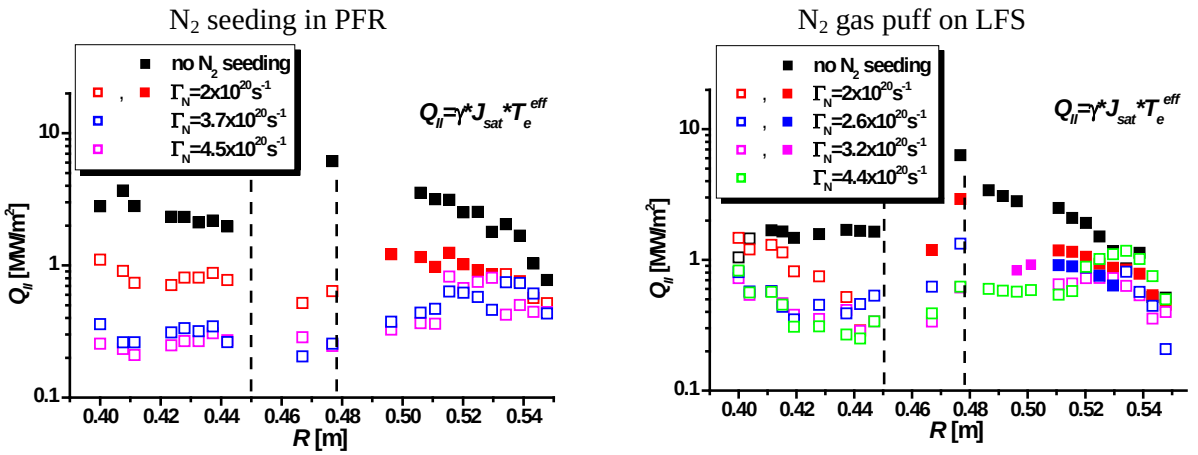

Figure 10. Poloidal distribution of the parallel power-flux density during N_2 seeding in the PFR (a) and on the LFS (b). The empty symbols denote the results when the EEDF is Maxwellian; the full, when the EEDF is bi-Maxwellian

3.2 Poloidal profiles of the plasma parameters during neon seeding on the LFS

Neon seeding was performed by using a valve placed on the LFS divertor region. The main problem in this experiment was the duration of the discharges, as the seeding cause a disruption. For example, figure 11 presents the poloidal profiles of the U_{fl}, U_{pl}, J_{sat} and T_e for 2.6×10^{20} neon molecules per second during discharge #15968. The different colors in the figures indicate data obtained at different times during the discharges. In black are the data in the time just before Ne was seeded; in red and blue, after seeding at times 1130 ms and 1150 ms, respectively. The floating potential decreased gradually during the seeding, and the poloidal distribution became flatter. The plasma potential was affected mostly in the divertor's HFS region, similarly to the case of nitrogen seeding.

After a 50-ms seeding, the J_{sat} peak at the outer strike point vanished. In the HFS divertor region and around the inner strike point, a Maxwellization of the electron distribution was observed, but the electron temperature around 3.5 eV was only maintained in the short interval between poloidal positions R = 0.40 m and R = 0.42 m. Around the outer strike point and the LFS divertor region, the EEDF remained bi-Maxwellian, although the temperature of the high-energy electron group decreased to 10 eV. During the Ne seeding, the temperature of the low-energy electron group was in the order of 3.5 eV. At the same time, Ne did not remain in the divertor region, but rather penetrated into the core plasma and cooled it [31].

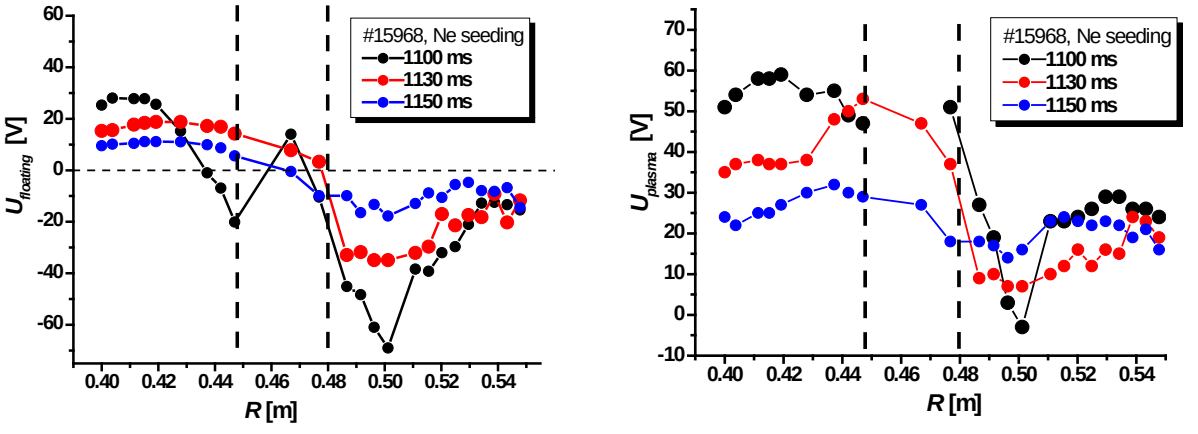

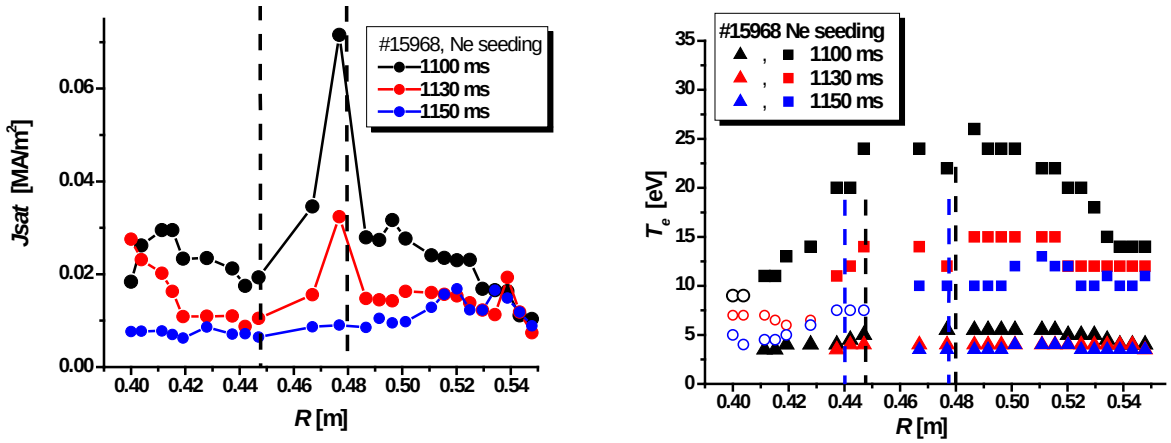

c) d)

Figure 11. Poloidal profiles of the floating (a) and plasma (b) potentials, the ion saturation current density (c) and the electron temperatures (d) at LFS gas puff during Ne seeding.

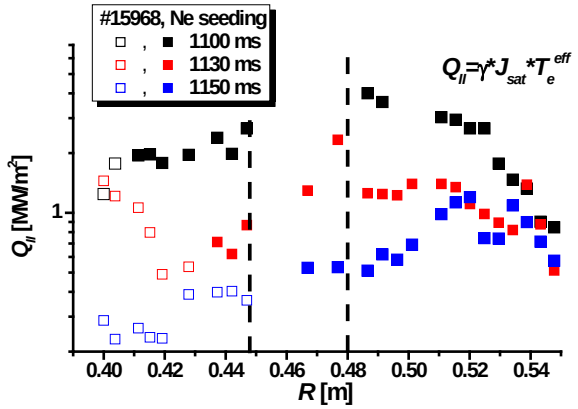

Figure 12. Time evolution of the parallel power-flux density poloidal distribution during Ne seeding. The empty symbols present the results when the EEDF is Maxwellian; the full, when the EEDF is bi-Maxwellian.

Figure 12 presents the time evolution of the poloidal profile of the parallel power flux density.

A decrease of $Q_{\parallel}$ by about one order of magnitude was observed on the HFS divertor region and in the vicinity of the strike points. In the far LFS divertor region, the changes during the time of seeding were much weaker.

Unfortunately, the neon seeded by a valve on the LFS accumulated in the core plasma and cooled it, which always resulted in a discharge disruption. It is, therefore, not suitable for the purpose of reaching a partial-detachment under our experimental conditions in the COMPASS tokamak.

4. Conclusions

This paper reports a study on nitrogen and neon impurity seeding in view of obtaining a semi-detachment mode in D-shaped, L-mode, deuterium plasmas. We explored the properties of the plasma in the divertor region before and during nitrogen and neon seeding by means of the 39 single graphite Langmuir probes embedded in the COMPASS tokamak divertor. The current-voltage probe characteristics measured were processed by the advanced first-derivative probe technique, which provides information on the poloidal distribution of the plasma potential and the real electron energy distribution function, respectively, the electron temperatures and densities. Using these data, the parallel power-flux density distribution was calculated in the divertor region of the COMPASS tokamak before and during the impurity seeding.

The probe measurements showed that, prior to impurity seeding, the EEDF in the divertor region of COMPASS tokamak is bi-Maxwellian with a low-energy electron population (4 – 6 eV) and a group of higher energy electrons (10 – 25 eV).

Nitrogen was seeded by valves placed on the private flux region and the low-field side in the divertor region. The impurity seeding led to Maxwellization of the plasma with electron temperature 5 – 7 eV, while the peaks on the strike points in the poloidal profiles of T_e, and J_{sat} disappeared during the seeding. The parallel power flux density dropped by about one order of magnitude.

The establishment of a Maxwellian EEDF in the divertor region due to the impurity seeding was faster when it was performed in the private flux region, but the confined plasma was cooled, the

discharge was shorter, not stable and ended with disruption. This is why we conclude that the nitrogen seeding in the private flux region is not effective in reaching a partial-detachment.

The Maxwellization of the plasma when the impurity puffing valve was on the LFS of the divertor region was slower and needed higher rates of impurity seeding; however, the discharges were stable and longer; thus, in this case the seeding was more effective in view of achieving a partial-detachment in the COMPASS tokamak.

Neon seeding by a valve on the LFS accumulated in the core plasma and cooled it, which always resulted in discharge disruption. It is, therefore, not suitable for the purpose of reaching a partial-detachment under our experimental conditions of the COMPASS tokamak.

Acknowledgements

This research has been partially supported by projects No. EF16_013/0001551, by the Joint Research Project between the Institute of Plasma Physics of the CAS and the Institute of Electronics BAS BG, by the Czech Science Foundation grant GA16-14228S, by MSMT project # LM2015045, by the co-fund under MEYS project # 8D15001, Slovenian Ministry of Education, Science and Sport (project P2-0073) and IAEA CRP F13019 - Research Contracts No 22727/R0 and No 22784/R0. This work has been carried out within the framework of the EUROfuison Consortium and has received funding from the Euratom research and training programme 2014-2018 and 2019-2020 under grant agreement No 633053. The views and opinions expressed herein do not necessarily reflect those of the European Commission.

References

[1] Krasheninnikov S. *et al* 2017 *J. Plasma Phys.* **83** 155830501
[2] Kallenbach A. *et al* 2010 *Plasma Phys. Control. Fusion* **52** 055002
[3] Asakura N. *et al* 2009 *Nucl. Fusion* **49** 15010
[4] Dumortier P. *et al* 2002 *Plasma Phys. Control. Fusion* **44** 1845
[5] Loarte A. *et al* 1998 *Nuclear Fusion* **38**/3 331
[6] LaBombard B. *et al* 1995 *Physics of Plasmas* **2** 2242
[7] Eich T. *et al* 2013 *J. Nucl. Mat.* **438** S72-S77
[8] Panek R. *et al* 2016 *Plasma Phys. Control. Fusion* **58** 014015
[9] Silva C.G. *et al* 2010 *Contrib. Plasma Phys.* **38** S1
[10] Dimitrova M. *et al* 2014 *Contrib. Plasma Phys.* **54** 255
[11] Dimitrova M. *et al* 2017 *44th EPS Conf. on Plasma Physics* (Belfast, Northern Ireland, 26 - 30 June 2017) P2.105
[12] Adamek J. *et al* 2017 *Nucl. Fusion* **57** 116017
[13] Komm M. *et al* 2017 *44th EPS Conf. on Plasma Physics* (Belfast, Northern Ireland, 26 - 30 June 2017) P1.118
[14] Weinzettl V. *et al* 2011 *Fus.Eng. Des.* **86** 1227
[15] Popov Tsv.K. *et al* 2016 *Plasma Sources Sci. Technol.* **25** 033001
[16] Hasan E. *et al* 2018 *JINST* **13** P04005
[17] Popov Tsv.K. *et al* 2015 *Plasma Phys. Control. Fusion* **57** 115011
[18] Mitov M. *et al* 2012 *J. Phys.: Conf. Series* **356** 012008
[19] Tagle J.A. *et al* 1987 *Plasma Phys. Control. Fusion* **29** 297
[20] Stangeby P.C. *et al* 1990 *Nuclear Fusion* **30** 1225
[21] Chodura R. 1992 *Contrib. Plasma Phys.* **32** 219
[22] Batishchev O.V. *et al* 1997 *Phys. Plasmas* **4** 1672
[23] Tskhakaya D. *et al* 2012 *Contrib. Plasma Phys.* **52** 490
[24] Popov Tsv. *et al* 2014 *Contrib. Plasma Phys*. **54** 267
[25] Jaworski M. *et al* 2013 *Journal of Nuclear Materials* **438** S384
[26] Godyak V. A. *et al* 2011 *J. Phys. D: Appl. Phys.***44** 233001
[27] Kovacic J. *et al* 2018 *45th EPS Conference on Plasma Physics* (Prague, Czech Republic, 2 - 6 July 2018) P1.1107
[28] Thrysøe A.S. *et al* 2016 *Plasma Phys. Control. Fusion* **58** 044010

[29] Itikawa Y. 2006 *Journal of Physical and Chemical Reference Data* **35** 31
[30] Stangeby P.C. 2000 *The Plasma Boundary of Magnetic Fusion Devices* (Bristol: Institute of Physics Publishing)
[31] Khodunov I. *et al* 2018 *poster at 28th Symposium on Plasma Physics and Technology* (Prague, Czech Republic, 18-21 June 2018)
[32] Silva C. *et al* 1999 *Journal Nucl. Mater.* **266-269** 679-684